Acta Crystallographica Section F
Structural Biology and Crystallization Communications
ISSN 1744-3091

The structure of *Staphylococcus aureus* phosphopantetheine adenylyltransferase in complex with 3′-phosphoadenosine 5′-phosphosulfate reveals a new ligand-binding mode

Hyung Ho Lee,[a]‡ Hye-Jin Yoon,[a]‡ Ji Yong Kang,[a] Ji Hyeon Park,[a] Do Jin Kim,[a] Kwang-Hyun Choi,[b] Seung-Kyu Lee,[b] Jinsu Song,[a] Hie-Joon Kim[a] and Se Won Suh[a,c]*

[a]Department of Chemistry, College of Natural Sciences, Seoul National University, Seoul 151-742, Republic of Korea, [b]ProMediTech, 1578-51 Shillim-dong, Kwanak-gu, Seoul 151-011, Republic of Korea, and [c]Department of Biophysics and Chemical Biology, College of Natural Sciences, Seoul National University, Seoul 151-742, Republic of Korea

‡ These authors contributed equally to this work.

Correspondence e-mail: sewonsuh@snu.ac.kr

Received 10 July 2009
Accepted 10 September 2009

PDB Reference: PAPS-bound *S. aureus* PPAT, 3f3m, r3f3msf.

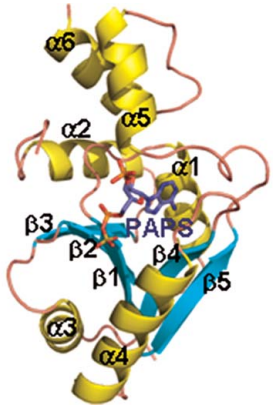

Bacterial phosphopantetheine adenylyltransferase (PPAT) catalyzes the penultimate step in the coenzyme A (CoA) biosynthetic pathway. It catalyzes the reversible transfer of an adenylyl group from ATP to 4′-phosphopantetheine (Ppant) to form dephospho-CoA (dPCoA) and pyrophosphate. Previous structural studies have revealed how several ligands are recognized by bacterial PPATs. ATP, ADP, Ppant and dPCoA bind to the same binding site in a highly similar manner, while CoA binds to a partially overlapping site in a different mode. To provide further structural insights into ligand binding, the crystal structure of *Staphylococcus aureus* PPAT was solved in a binary complex with 3′-phosphoadenosine 5′-phosphosulfate (PAPS). This study unexpectedly revealed a new mode of ligand binding to PPAT, thus providing potentially useful information for structure-based discovery of inhibitors of bacterial PPATs.

1. Introduction

Coenzyme A (CoA) is an essential cofactor in numerous biosynthetic, degradative and energy-yielding metabolic pathways and is required in several key reactions in intermediary metabolism (Leonardi *et al.*, 2005; Geerlof *et al.*, 1999). In bacteria, it is synthesized in five steps from pantothenate (vitamin B_5), cysteine and ATP (Robishaw & Neely, 1985). Phosphopantetheine adenylyltransferase (PPAT), a member of the nucleotidyltransferase superfamily (Bork *et al.*, 1995), catalyzes the penultimate step in this biosynthetic pathway: the reversible transfer of an adenylyl group from ATP to 4′-phosphopantetheine (Ppant), yielding dephospho-CoA (dPCoA) and pyrophosphate (Izard & Geerlof, 1999). In mammals, PPAT and dephospho-CoA kinase occur as a bifunctional enzyme called CoA synthase (Aghajanian & Worrall, 2002). Bacterial PPATs and mammalian PPATs are highly dissimilar in primary sequence, thus making the bacterial PPATs an attractive target for the discovery of antibacterials.

Escherichia coli PPAT has been the target of extensive structural studies. Its structures in complex with dPCoA (Izard & Geerlof, 1999), ATP (Izard, 2002), Ppant (Izard, 2002) and CoA (Izard, 2003) have been reported. It is a homohexamer with 32 point-group symmetry. Only one trimer within the *E. coli* PPAT hexamer binds Ppant (Izard, 2002) or dPCoA (Izard & Geerlof, 1999), whereas both trimers bind ATP (Izard, 2002). Superposition of the bound adenylyl moieties of dPCoA and ATP in *E. coli* PPAT suggests an in-line displacement mechanism involving nucleophilic attack by Ppant on the α-phosphate of ATP (Izard & Geerlof, 1999; Izard, 2002). The conserved His18 of the T*X*GH sequence motif in *E. coli* PPAT plays an essential role in stabilizing the pentacovalent transition state, while Thr10 and Lys42 have been shown to orient the nucleophile of Ppant for attack on the α-phosphate of ATP (Izard, 2002). The structure of *E. coli* PPAT bound to CoA, a feedback regulator, revealed that the binding of the adenylyl moiety of CoA does not overlap with the adenylyl-binding site of dPCoA (Izard, 2003). The 3′-phosphate on the ribose is required for the binding of CoA in this novel conformation (Izard, 2003). The structures of *Mycobacterium tuberculosis* PPAT in the apo form (Morris & Izard, 2004), *Thermus thermophilus* PPAT in complex with Ppant (Takahashi *et al.*, 2004),

Table 1
Statistics of data collection and refinement.

Values in parentheses are for the highest resolution shell.

Data-collection statistics	
X-ray wavelength (Å)	0.97880
Space group	$P6_322$
Unit-cell parameters (Å)	$a = b = 66.89$, $c = 124.14$
Resolution range (Å)	30–2.40 (2.44–2.40)
Total/unique reflections	44759/6551 (1618/292)
Completeness (%)	94.3 (92.1)
Average $I/\sigma(I)$	27.3 (4.3)
R_{merge}† (%)	9.9 (41.7)
Model-refinement statistics	
R_{work}/R_{free}‡ (%)	20.3/26.3
No. of non-H atoms	
Protein	1252
Water	43
PAPS	31
Average B factor (Å^2)	
Protein	28.6
Water	28.2
PAPS	40.8
R.m.s. deviations from ideal geometry	
Bond lengths (Å)	0.0066
Bond angles (°)	1.32
MolProbity protein-geometry analysis	
Ramachandran favoured (%)	98.67
Ramachandran allowed (%)	1.33
Ramachandran outliers (%)	0.00
MolProbity score	2.18

† $R_{merge} = \sum_{hkl}\sum_i |I_i(hkl) - \langle I(hkl)\rangle|/\sum_{hkl}\sum_i I_i(hkl)$, where $I(hkl)$ is the intensity of reflection hkl, $\sum_{hkl}$ is the sum over all reflections and $\sum_i$ is the sum over i measurements of reflection hkl. ‡ $R = \sum_{hkl}\big||F_{obs}| - |F_{calc}|\big|/\sum_{hkl}|F_{obs}|$; R_{free} is calculated for a randomly chosen set (~5%) of reflections which were not used for structure refinement and R_{work} is calculated for the remaining reflections.

and *Bacillus subtilis* PPAT in complex with ADP (Badger *et al.*, 2005) have also been reported. Futhermore, the structures of an archaeal PPAT (PDB code 3do8; R. Zhang, R. Wu, R. Jedrzejczak & A. Joachimiak, unpublished work) and a mammalian bifunctional coenzyme A synthase covering the C-terminal third of PPAT and the whole dephospho-CoA kinase (PDB code 2f6r; Joint Center for Structural Genomics, unpublished work) have been solved.

Staphylococcus aureus, a Gram-positive pathogen, is a major cause of hospital- and community-acquired infections. The development of methicillin resistance and more recently vancomycin resistance in *S. aureus* poses a serious health problem. Based on the inhibitor-bound structure of *E. coli* PPAT, a potent and specific inhibitor with an IC_{50} of 6 n*M* against *E. coli* PPAT but no activity against porcine PPAT has been obtained (Zhao *et al.*, 2003). To aid in structure-based discovery of new antibacterial compounds against major human pathogens such as *S. aureus*, detailed structural information on the binding modes of different ligands to the PPAT active site is desirable. In this study, we have solved the crystal structure of *S. aureus* PPAT as a binary complex with 3′-phosphoadenosine 5′-phosphosulfate (PAPS). This represents the first structure of PPAT complexed with PAPS. The PAPS-binding site overlaps with that of ATP, but their binding modes are distinct from each other. Thus, our structural study has unexpectedly revealed a new mode of ligand binding to PPAT, thus providing potentially useful information for the structure-based discovery of new antibacterial agents against PPATs.

2. Materials and methods

2.1. Protein expression, purification and crystallization

The *coaD* gene (SA_0973) encoding *S. aureus* PPAT was cloned into the expression vector pET-21a(+) (Novagen) using the *Nde*I/*Xho*I sites. This vector construction adds an eight-residue tag (LE-HHHHHH) to the C-terminus of the gene product to facilitate protein purification. The protein was overexpressed in *E. coli* C41 (DE3) cells using Luria–Bertani culture medium. Following growth to mid-log phase at 310 K, protein expression was induced with 1 m*M* IPTG and the cells were incubated for an additional 18 h at 291 K. The cells were then lysed by sonication in lysis buffer (20 m*M* Tris–HCl pH 7.9 and 500 m*M* NaCl) containing 50 m*M* imidazole. Following centrifugation at 3800*g* for 60 min, the supernatant was applied onto a nickel–nitrilotriacetic acid–agarose affinity-chromatography column (Qiagen). The protein was eluted with buffer *A* containing 500 m*M* imidazole. The supernatant was applied onto a HiLoad XK-16 Superdex 200 prep-grade column (GE Healthcare) previously equilibrated with buffer *A* (50 m*M* Tris–HCl pH 8.0 containing 100 m*M* NaCl). Finally, the purified enzyme was concentrated to 26 mg ml^{-1} using a YM10 ultrafiltration membrane (Amicon) and stored at 203 K. *S. aureus* PPAT was crystallized by the hanging-drop vapour-diffusion method at 297 K by mixing equal volumes (2 µl each) of protein solution (26 mg ml^{-1} in buffer *A*) and reservoir solution (100 m*M* imidazole pH 8.0, 0.9–1.2 *M* potassium/sodium tartrate and 0.2 *M* NaCl). The crystals grew to approximate dimensions of 0.2 × 0.2 × 0.1 mm within a few days.

2.2. X-ray data collection and structure determination

Crystals were frozen using a cryoprotectant solution consisting of 20%(*w*/*v*) polyethylene glycol 400 in the crystallization mother liquor. X-ray diffraction data were collected at 100 K on an Area Detector Systems Corporation Quantum 4R CCD detector at the experimental station BL-18B of Photon Factory, Japan. For each image, the crystal was rotated by 1°. The raw data were processed and scaled using the *HKL*-2000 program suite (Otwinowski & Minor, 1997). Table 1 summarizes the statistics of data collection. The crystal was indexed in space group $P6_322$, with unit-cell parameters $a = b = 66.89$, $c = 124.14$ Å, $\alpha = \beta = 90$, $\gamma = 120°$ (Table 1). A monomer is present in the asymmetric unit, giving a crystal volume per protein mass (V_M) of 2.06 Å^3 Da^{-1} and a solvent content of 40.4%.

The structure was solved by the molecular-replacement method using the monomer model of *E. coli* PPAT (PDB code 1b6t; Izard & Geerlof, 1999). A cross-rotational search followed by a translational search was performed using the program *CNS* (Brünger *et al.*, 1998; Brunger, 2007). Subsequent manual model building was performed

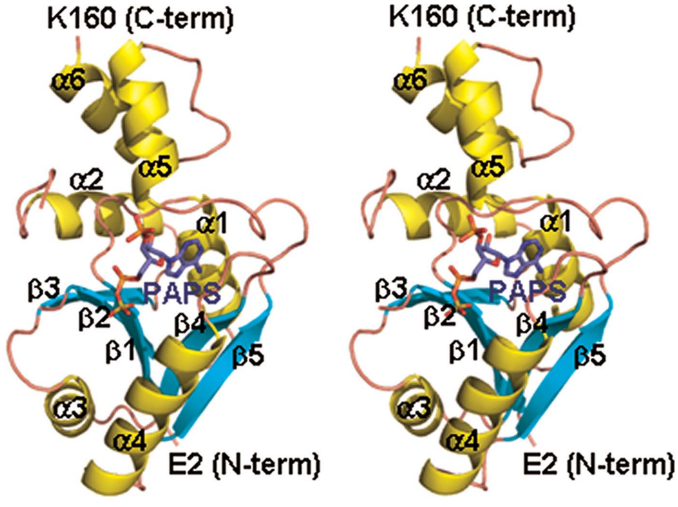

Figure 1
Stereo ribbon diagram of *S. aureus* PPAT monomer. PAPS bound in the active site is shown as a stick model.

using the program *O* (Jones *et al.*, 1991). The model was refined by minimizing the maximum-likelihood target function on amplitudes using the program *CNS* (Brünger *et al.*, 1998; Brunger, 2007), including bulk-solvent correction. Several rounds of model building, simulated annealing, positional refinement and individual *B*-factor refinement were performed. The model has reasonable stereochemistry as evaluated using the program *MolProbity* (Davis *et al.*, 2007). Refinement statistics are summarized in Table 1.

3. Results and discussion

3.1. Monomer and hexamer structures

We have determined the crystal structure of *S. aureus* PPAT in complex with PAPS at 2.40 Å resolution. The refined model includes residues 2–39 and 45–160 of one PPAT monomer in the asymmetric unit. The N-terminal methionine, an eight-residue fusion tag at the C-terminus and residues 40–44 of the recombinant enzyme are presumably disordered in the crystal. The monomer adopts the dinucleotide-binding fold (or the canonical Rossmann fold; Rossmann *et al.*, 1975). Its core contains a five-stranded parallel β-sheet arranged in the order $\beta3$-$\beta2$-$\beta1$-$\beta4$-$\beta5$, which is packed on one side by four α-helices ($\alpha1$, $\alpha2$, $\alpha5$ and $\alpha6$) and on the other side by two α-helices ($\alpha3$ and $\alpha4$) (Fig. 1). *S. aureus* PPAT is hexameric and displays 32 symmetry like other bacterial PPATs (Izard & Geerlof, 1999; Izard, 2002, 2003; Morris & Izard, 2004; Takahashi *et al.*, 2004; Badger *et al.*, 2005). All six subunits of *S. aureus* PPAT are bound with PAPS. This is similar to the structures of *T. thermophilus* PPAT in complex with Ppant (Takahashi *et al.*, 2004) and *B. subtilis* PPAT in complex with ADP (Badger *et al.*, 2005). In contrast, in the *E. coli* PPAT structures Ppant and dPCoA were bound in only one of the two trimeric units (Izard & Geerlof, 1999; Izard, 2002). A structural comparison of *S. aureus* PPAT with mammalian PPATs is not possible because little structural information is available on mammalian PPATs apart from the C-terminal third of mouse PPAT (PDB code 2f6r; Joint Center for Structural Genomics, unpublished work).

Table 2
Interactions of PAPS with *S. aureus* PPAT.

Protein–ligand contacts	Distance (Å)
Ser11 N–PAPS O4P	2.82
Ser11 N–PAPS O5P	3.07
His19 NE2–PAPS O2	3.18
Arg89 NH2–PAPS OS2	2.88
Arg92 NH1–PAPS O4	3.01
Tyr99 OH–PAPS OS2	2.98
Ser129 OG–PAPS O1P	3.13
Ser130 OG–PAPS O2	3.03
Ser131 N–PAPS O3P	2.43
Ser131 OG–PAPS O3P	2.45
Wat1–PAPS O2	2.99
Wat2–PAPS O4P	2.72
Wat24–PAPS OS1	2.40
Wat44–PAPS N7	3.25

3.2. 3′-Phosphoadenosine 5′-phosphosulfate binds in a distinct mode

Although we did not add any ligand during the crystallization of *S. aureus* PPAT, the ($F_o - F_c$) map calculated using the refined model revealed clear electron density for a bulky ligand in the ATP-binding pocket of the active site. The extra electron density could best be

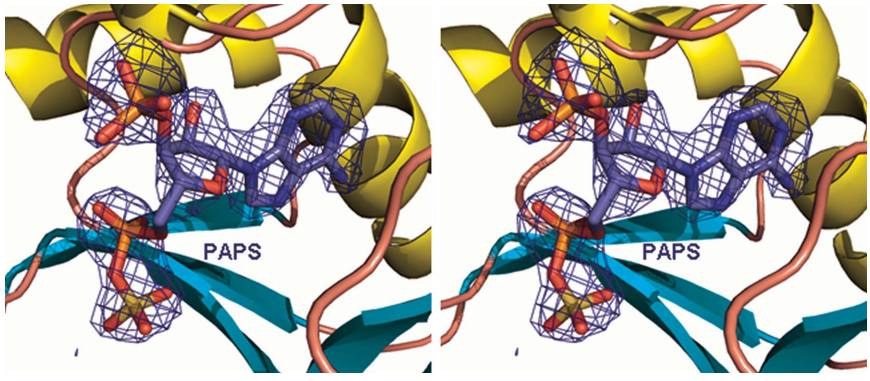

Figure 2
$F_o - F_c$ OMIT electron-density map of PAPS contoured at the 2.5σ level. The mean *B* factor of PAPS (40.8 Å^2) is slightly higher than that of the protein atoms, suggesting that the occupancy of PAPS is slightly lower than one. When the occupancy of PAPS is fixed at 0.8, its *B* factor (30.9 Å^2) is comparable to that of the protein atoms (28.6 Å^2).

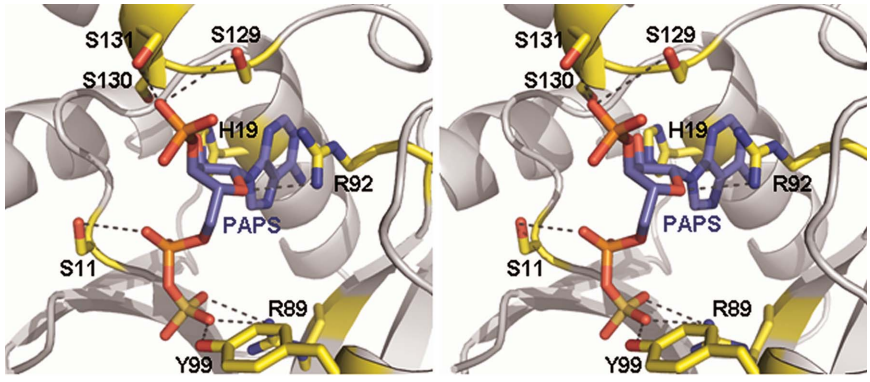

Figure 3
Stereoview of the active site around the bound PAPS.

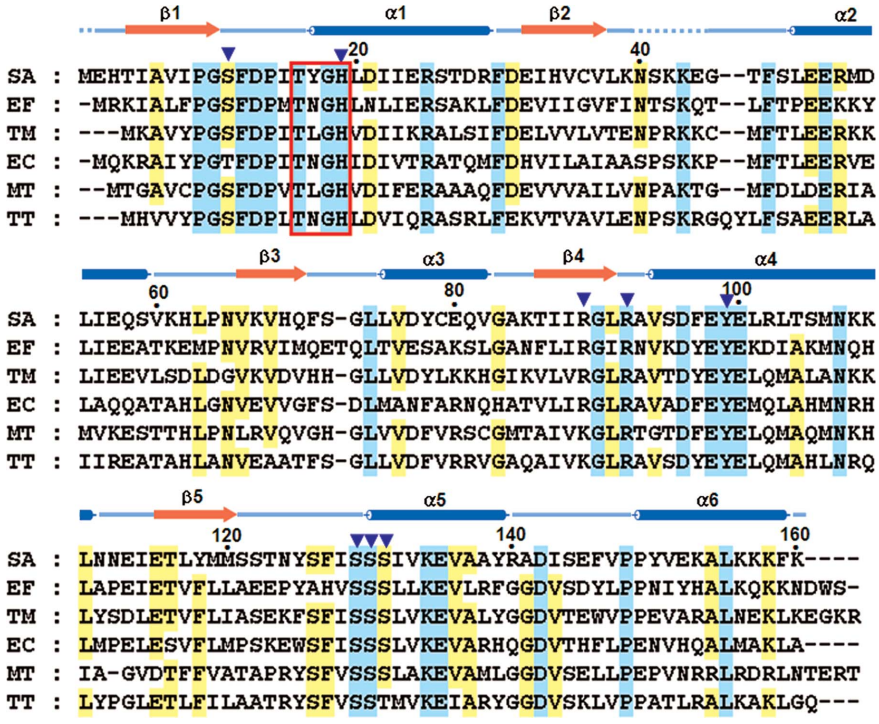

Figure 4
Alignment of bacterial PPAT amino-acid sequences. SA, *Staphylococcus aureus* (SWISS-PROT accession code P63819); EF, *Enterococcus faecalis* (Q831P9); TM, *Thermotoga maritima* (Q9WZK0); EC, *Escherichia coli* (P0A6I6); MT, *Mycobacterium tuberculosis* (P0A530); TT, *Thermus thermophilus* (Q72K87). Strictly conserved residues and semi-conserved residues are coloured cyan and yellow, respectively. The T*X*GH sequence motif is enclosed in a red box. The residues of *S. aureus* PPAT that interact with PAPS are indicated by blue inverted triangles above the sequences. Cylinders and arrows above the sequences denote α-helices and β-strands, respectively. Secondary-structure elements are indicated for the PAPS complex of *S. aureus* PPAT. This figure was produced using *ClustalX* (Thompson *et al.*, 1997) and *GeneDoc* (http://www.nrbsc.org/).

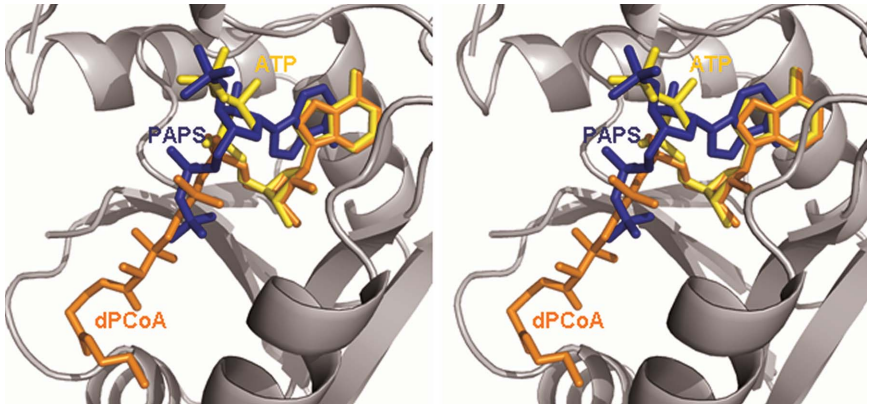

Figure 5
The distinct mode of PAPS (blue) binding to *S. aureus* PPAT. ATP (yellow, 1gn8 chain *B*) and dPCoA (orange, 1b6t chain *B*) bound in *E. coli* PPAT (Izard & Geerlof, 1999; Izard, 2002) are positioned in the active site of *S. aureus* PPAT by superimposing PPAT monomer structures. With the exception of Fig. 4, all figures were produced using *PyMOL* (http://www.pymol.org).

interpreted as PAPS (Fig. 2). Fitting with ATP was much less satisfactory. Apparently, endogenous PAPS inside the *E. coli* cells bound to the recombinant *S. aureus* PPAT. PAPS is a co-substrate for sulfuryl transferases and is a ubiquitous intracellular cofactor (Klaassen & Boles, 1997). In the PAPS complex of *S. aureus* PPAT, Arg89 and Tyr99 interact with the sulfate moiety of the 5′-phosphosulfate group of PAPS, while Ser11 interacts with the phosphate moiety of the 5′-phosphosulfate group. Ser129 and Ser131 interact with the 3′-phospho group. His19, Arg92 and Ser130 interact with ribose (Fig. 3 and Table 2). All these residues are well conserved in bacterial PPATs (Fig. 4). In conclusion, PAPS is bound in the ATP-binding pocket of *S. aureus* PPAT in a mode that is distinct from those of either ATP (Izard, 2002) or the adenylyl moiety of dPCoA (Izard & Geerlof, 1999) bound to *E. coli* PPAT (Fig. 5). The new ligand-binding mode revealed in this study should be useful in the design of PPAT inhibitors because PAPS may be a potential inhibitor of bacterial PPATs.

We thank the beamline staff for assistance during data collection at the BL-18B experimental station of Photon Factory, Tsukuba, Japan. This work was supported by Korea Ministry of Education, Science and Technology (MEST), the National Research Foundation of Korea (NRFK) through the Basic Science Outstanding Scholars

Program and the Innovative Drug Research Center (IDRC) for Metabolic and Inflammatory Disease (grant No. R11-2007-107-00000-0).

References

Aghajanian, S. & Worrall, D. M. (2002). *Biochem. J.* **365**, 13–18.
Badger, J. *et al.* (2005). *Proteins*, **60**, 787–796.
Bork, P., Holm, L., Koonin, E. V. & Sander, C. (1995). *Proteins*, **22**, 259–266.
Brunger, A. T. (2007). *Nature Protoc.* **2**, 2728–2733.
Brünger, A. T., Adams, P. D., Clore, G. M., DeLano, W. L., Gros, P., Grosse-Kunstleve, R. W., Jiang, J.-S., Kuszewski, J., Nilges, M., Pannu, N. S., Read, R. J., Rice, L. M., Simonson, T. & Warren, G. L. (1998). *Acta Cryst.* D**54**, 905–921.
Davis, I. W., Leaver-Fay, A., Chen, V. B., Block, J. N., Kapral, G. J., Wang, X., Murray, L. W., Arendall, W. B. III, Snoeyink, J., Richardson, J. S. & Richardson, D. C. (2007). *Nucleic Acids Res.* **35**, W375–W383.
Geerlof, A., Lewendon, A. & Shaw, W. V. (1999). *J. Biol. Chem.* **274**, 27105–27111.
Izard, T. (2002). *J. Mol. Biol.* **315**, 487–495.
Izard, T. (2003). *J. Bacteriol.* **185**, 4074–4080.
Izard, T. & Geerlof, A. (1999). *EMBO J.* **18**, 2021–2030.
Jones, T. A., Zou, J.-Y., Cowan, S. W. & Kjeldgaard, M. (1991). *Acta Cryst.* A**47**, 110–119.
Klaassen, C. D. & Boles, J. W. (1997). *FASEB J.* **11**, 404–418.
Leonardi, R., Zhang, Y.-M., Rock, C. O. & Jackowski, S. (2005). *Prog. Lipid Res.* **44**, 125–153.
Morris, V. K. & Izard, T. (2004). *Protein Sci.* **13**, 2547–2552.
Otwinowski, Z. & Minor, W. (1997). *Methods Enzymol.* **276**, 307–326.
Robishaw, J. D. & Neely, J. R. (1985). *Am. J. Physiol.* **248**, E1–E9.
Rossmann, M. G., Liljas, A., Brändén, C. I. & Banaszak, L. J. (1975). *The Enzymes*, 3rd ed., edited by P. D. Boyer, Vol. XI, pp. 61–102. London: Academic Press.
Takahashi, H., Inagaki, E., Fujimoto, Y., Kuroishi, C., Nodake, Y., Nakamura, Y., Arisaka, F., Yutani, K., Kuramitsu, S., Yokoyama, S., Yamamoto, M., Miyano, M. & Tahirov, T. H. (2004). *Acta Cryst.* D**60**, 97–104.
Thompson, J. D., Gibson, T. J., Plewniak, F., Jeanmougin, F. & Higgins, D. G. (1997). *Nucleic Acids Res.* **25**, 4876–4882.
Zhao, L., Allanson, N. M., Thomson, S. P., Maclean, J. K., Barker, J. J., Primrose, W. U., Tyler, P. D. & Lewendon, A. (2003). *Eur. J. Med. Chem.* **38**, 345–349.